Photoinduced Formation of H-bonded Ion Pair in HCFC-133a

Gessenildo Pereira Rodrigues, Thayana Maria Lopes de Lima, Railton Barbosa de Andrade, Gessenildo Pereira Rodrigues, Thayana Maria Lopes de Lima, Railton Barbosa de Andrade, Elizete Ventura, Silmar Andrade Do Monte, Mario Barbatti

Photoinduced Formation of H-bonded Ion Pair in HCFC-133a

Gessenildo Pereira Rodrigues[1,2], Thayana Maria Lopes de Lima[1], Railton Barbosa de Andrade [1], Elizete Ventura[1], Silmar Andrade do Monte[1*], Mario Barbatti[3*]

[1]*Universidade Federal da Paraíba, 58059-900, João Pessoa-PB, Brazil.*

[2]*Faculdade Rebouças, 58406-040, Campina Grande-PB, Brazil.*

[3]*Aix Marseille Univ, CNRS, ICR, Marseille, France.*

Abstract. High-level multireference electronic structure calculations have been performed to study the Cl^- yield from photoexcited CF_3CH_2Cl (HCFC-133a). The analysis of this process tells that it relates to an electron transfer from the carbon to the Cl atom, forming a highly polar contact ion-pair complex, $CF_3HCH^+\cdots Cl^-$, in the excited (S_3) state. This complex has a strong binding energy of 3.53 eV, from which 0.47 eV is due to an underlying hydrogen bond. Through comparison with the results obtained for the prototype CH_3Cl system, where a similar ion-pair state associated with Cl^- formation has also been observed, it is suggested that photodissociation of HCFC-133a can also yield Cl^- through analogous process. This hypothesis is further supported by nonadiabatic dynamics simulations, which shows formation of the ion-pair complex in the sub-picosecond time scale.

Introduction

Compared to chlorofluorocarbons (CFCs), hydrochlorofluorocarbons (HCFCs) are much less harmful to the ozone layer, mainly due to their degradation by reactions with OH radicals in the troposphere.[1] Nevertheless, as the HCFCs are important greenhouse-effect gases,[2] they have been included in the Kyoto protocol,[3] which aims to stop their production until 2020.[4-8] HCFC-133a (CF_3CH_2Cl) has been used in the pharmaceutical industry and also as a precursor of the HFC-134a (CF_3CH_2F).[9, 10] It was first detected in the atmosphere four years ago, by Laube *et. al.*[11] More recently, McGillen e*t. al.*[12] have evaluated several parameters of HCFC-133a with important atmospheric implications.

Ground state reactions of HCFC-133a have been studied by several authors. Three thermal reaction channels, induced using the infrared multiphoton absorption technique, have been studied by Setser *et. al.*,[13] and Rakestraw and Holmes[14] measured the rate constants for these three reactions. Enstice *et. al.*[15] studied HCFC-133a formation from CF_2ClCH_2F* molecules, while Wang *et. al.*[16] and Zhao *et. al.*[17] have studied its hydrogen abstraction reactions by F and Cl atoms, respectively, through direct dynamics calculations. More recently, McGillen e*t. al.*[12] have studied the rate coefficient of its reaction with OH.

On the other hand, studies concerning its photochemical reactions are much scarcer. To the best of our knowledge, there is only one experimental study involving primary photochemical processes for the HCFC-133a molecule.[18] Two wavelengths (at 123.6 and 147 nm) have been used, and molecular as well as halogen elimination have been observed.[18] The quantum yields of molecular processes increase with photon energy, due to the preferential formation of a Rydberg state.[18] Our group performed the first excited-state calculations for the vertical excitation of HCFC-133a, at the MR-CISD level in the range up to 9.8 eV.[19] Later, our group performed nonadiabatic dynamics calculations at the TDDFT level starting at the 10 ± 0.25 eV spectral window,[20] to compare to the experimental results obtained by Ichimura *et. al.* after 123.6 nm excitation.[18] The main experimental channel, Cl + F elimination, should preferentially take place through Cl dissociation in the excited state followed by F dissociation in the ground state, while the second main experimental channel (Cl + H) are mainly due to excited-state fragmentation.[20] While the third channel (F + H) should have a partial

contribution from ground-state fragmentation. CC bond fission are expected to take place exclusively in the excited state, followed by recombination in the ground state.[20]

Now, we focus on the elimination of Cl^- anion from HCFC-133a. The experimental data from ref. [18] does not make clear how much of the Cl elimination is due to such charged species. Nevertheless, in the closely related system CH_3Cl, Cl^- is the dominant anion formed, and its most intense peak is in the region from 10.5 to 11.9 eV, as revealed by the vacuum-UV photoexcitation (in the range from 8 to 35 eV) investigations by Tuckett *et al.*[21, 22] In particular, due to the linear dependence of its signal with pressure, the authors concluded that Cl^- (and the other anions studied) arises from ion-pair formation instead of from dissociative electron attachment.[21, 22] Recently, our group characterized[23] the photochemical formation of such a transient H-bonded ion pair for the CH_3Cl, with a structure represented by $H_2CH^+\cdots Cl^-$, during the predissociation of Cl^- (reaction (1)). Due to the substantial similarity between the electronic properties of CF_3CH_2Cl and CH_3Cl (these similarities are discussed later in this work), it is likely that Cl^- fragments are yielded from HCFC-133a through an ion-pair state analogous to that of CH_3Cl (reaction (2)).

$$CH_3Cl \xrightarrow{h\nu} \left[H_2CH^+\cdots Cl^-\right]^* \rightarrow H_2CH^+ + Cl^- \quad (1)$$

$$CF_3CH_2Cl \xrightarrow{h\nu} \left[CF_3HCH^+\cdots Cl^-\right]^* \rightarrow CF_3CH_2^+ + Cl^- \quad (2)$$

In the present work, multireference configuration interactions with singles and doubles plus size-extensivity corrections (MR-CISD+Q) is used to map fourteen excited states of CF_3CH_2Cl, including valence and Rydberg states. Emphasis is given to nonadiabatic relaxation pathways along the C–Cl coordinate, which can lead to an ion-pair whose structure is like that found for CH_3Cl. The same types of excited states involved in the ion-pair formation of CH_3Cl are obtained here. The properties of the $CF_3HCH^+\cdots Cl^-$ ion pair are discussed in detail and compared to those of the $H_2CH^+\cdots Cl^-$ ion-pair.

To check the hypothesis that the population of the $CF_3HCH^+\cdots Cl^-$ ion pair state could be a primary source of Cl^- fragments, on-the-fly non-adiabatic mixed quantum-classical dynamics,[24] starting from the $\sigma 4p_\sigma$ state, is also performed. The choice of this state arises from comparison with CH_3Cl, for which, among all computed states in ref.[23], the $\sigma 3p_\sigma$ state is the one which is expected to lead to the ion-pair channel with maximum

probability. Due to the exceedingly high computational costs of such simulations, they are not affordable at the MR-CISD levels employed in the discussion of the potential energy curves. Although they could have been done at MCSCF level with some smaller basis set, the lack of electron dynamic correlation would have led to unreliable results. Therefore, for the dynamics simulations, we resorted to an entirely distinct electronic-structure methodology, the linear-response time-dependent density functional theory (TDDFT).

The results from the potential energy mapping and dynamics simulations led to a picture where the high-energy excitation of HCFC-133a triggers a cascade of nonadiabatic events, which significantly populate an ion-pair state and yield Cl^- fragments.

2. Computational details

First, the ground state geometry of HCFC-133a has been optimized at the MP2 level with the aug-cc-pVTZ basis set.[25] Then, a relaxed scan along the C–Cl coordinated has been performed at the same level, from 1.766 to ~3.6 Å. At the obtained structures, single-point calculations at the multiconfigurational self-consistent field (MCSCF) and MR-CISD levels have then been done to map the fifteen lowest singlet states. C_s symmetry has been used for the potential energy profiles. Previous calculations performed for the CF_3Cl molecule indicate that the spin-orbit couplings for this type of molecule is small, about 0.009 eV.[26] Therefore, as our focus is the ultrafast (sub-picosecond) relaxation, we restricted the investigations to the singlet manifold.

The symmetry plane is the xy plane. The initial molecular orientation is shown in Figure 1. The Cl atom 3p lone pair along the C–Cl axis is named $3p_\sigma$, and its interaction with the singly occupied $2p_\sigma$(C) orbital of the CF_3CH_2 radical leads to the bonding and anti-bonding σ and σ^* orbitals. The symmetric and anti-symmetric Cl lone pairs are designated as n_1 and n_2, respectively. The set of ns, np_σ, and the (np_1,np_2) pair of Rydberg orbitals have also been included. All These orbitals are shown in Table S4 of the Supporting Information.

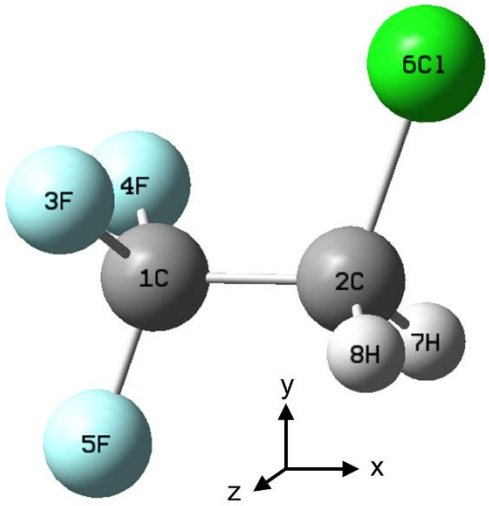

Figure 1. Initial molecular orientation used for the calculation of the vertical states and also as the starting point for generating the relaxed geometries used for the subsequent potential energy curves calculations.

For the single-point calculations, the *ref1* space defined in Table 1 has been used at the MCSCF and MR-CISD levels. The complete active space (CAS) at the MCSCF level has been chosen to comprise 6 electrons (four from the two n orbitals and two from the σ bond). The σ* orbital has also been included in the CAS, while the four Rydberg orbitals (ns, np_σ, and the (np_1, np_2) pair) have been added to the auxiliary (AUX) space, with the restriction that only single CAS → AUX excitations are allowed. Fifteen (9A′ and 6A″) singlet states with equal weights have been included in the state-averaged MCSCF calculations.

Table 1. Active and reference spaces used for the species studied in this manuscript. When it is the case, only CAS → AUX excitations have been employed.

Reference space	MCSCF		MR-CISD	
	CAS	AUX	CAS	AUX
valence	n_1, n_2, σ, σ*	----	n_1, n_2, σ, σ*	----
ref1	n_1, n_2, σ, σ*	ns, np_σ, np_1, np_2	n_1, n_2, σ, σ*	ns, np_σ, np_1, np_2

Full geometry optimizations have been performed for the $3^1A'$ (the ion-pair) state, at the MR-CISD level, using the valence space at both MR-CISD and MCSCF

levels (see Table 1). The absence of Rydberg orbitals, in this case, is justified by the significant energy difference between the ion-pair and the next high-lying state (an n3s Rydberg, see Figure 2). For the valence space, four (3A′ and 1A″) singlet states with equal weights have been included in the state-averaged MCSCF calculations.

At the MR-CISD level, the low-lying orbitals at the ground state geometry are divided into two subsets, that is, the frozen-core (FC) and the valence orbitals. The former set includes the K (for the C and F atoms) and K + L (for the Cl atom) shells, while the second set consists of the doubly occupied valence orbitals. Previous calculations on similar systems indicate that the L shell of the Cl atom has virtually negligible importance on the excited states' properties.[26, 27] The doubly occupied orbitals remain with fixed (that is, equals two) occupation numbers only in the reference configurations, while the FC orbitals remain doubly occupied in the reference as well as in the excited CSF space.

The reference configuration state functions (CSF) are then used to generate the excited CSF space through single and double excitations from all internal (active + doubly occupied) into all virtual orbitals, at the MR-CISD level. The final CSF space comprises the reference and the excited CSFs. In generating this last MR-CISD expansion, the interactive space restriction has been used.[28] The Davidson correction extended to the multi-reference case (+Q) has been used to account for the size-extensivity error.[29, 30]

The purpose of choosing *ref1* space is to get a correct description of the fifteen studied states in the region of the potential energy curves only up to a C–Cl distance compatible with the formation of the ion-pair, ~ 3.6 Å. A description of these states until complete dissociation requires the inclusion of additional states and orbitals.[23, 31] On the other hand, the *valence* space is adequate for a correct description of the ion-pair and its lower-lying states, $1^1A'$, $2^1A'$ and $1^1A''$, from ~ 2.6 Å to its complete dissociation.

The cation fragment $[CF_3CH_2]^+$, necessary to obtain the dissociation limit of the ion-pair channel, has been treated using an active space (at both CASSCF and MR-CISD levels) consisting of five orbitals, that is, the three lone pair orbitals of the F atom in the symmetry plane, along with the $2p_\sigma$ orbitals of both C atoms. This choice is due to the F migration, from C1 to C2, observed at correlated levels.[32] These orbitals are shown in Table S5 of the Supporting Information. Three (2A′ and 1A″) singlet states with equal weights have been included in the state-averaged CASSCF calculations. After geometry optimization of the $[CF_3CH_2]^+$ fragment, the Cl atom was placed at a distance of 50 Å

from the charge-center (the C1 atom, as the final optimized structure is $[CF_2CFH_2]^+$ due to F migration) and collinear with both C atoms. This supermolecule has then been used to obtain the dissociation limit of the ion-pair channel (with the *valence* space). The residual Coulomb energy between the charged species (0.29 eV at 50 Å) was further discounted from the potential energy of the supermolecule.

The aug-cc-pVTZ basis set[25] has been used at the MP2 level, while the MR-CISD potential energy curves have been computed with the mixed d-aug-cc-pVTZ(Cl)/aug-cc-pVDZ(C,H,F) basis set (named B1 from here on). This basis set has been shown to be flexible enough to handle localization of the Rydberg orbitals either in the Cl or in the C2 atom, a necessary requisite, as such localization changes with the C–Cl distance. Geometry optimizations of the $[CF_3CH_2]^+$ fragment in the ground and ion-pair states have been performed with the mixed aug-cc-pVDZ(C,F)/cc-pVTZ(H,Cl) basis set (B2 basis set). Single-point calculations on the supermolecule in the ground and ion-pair state geometries have been performed with the mixed aug-cc-pVTZ(C,H,Cl)/cc-pVTZ(F) basis set (B3 basis set). Details on the basis set choice are discussed in the Supporting Information (SI-7).

Nonadiabatic dynamics simulations were carried out to address the possibility of reaching the ionic channel from the $\sigma 4p_\sigma$ state. These simulations were performed as explained in ref.[20], that is, using decoherence-corrected fewest-switches surface hopping[33, 34] at the TDDFT level[31, 35] with the ωB97XD functional.[36] The only difference is that in the present work a spectral window at 11.2±0.25 eV has been chosen for the initial excitation, which corresponds to a window centered at the vertical excitation energy of the $\sigma 4p_\sigma$ state, obtained at the TDDFT/ωB97XD level with the d-aug-cc-pVDZ(Cl)/aug-cc-pVDZ(H,C,F) basis set (B4 basis set). One hundred initial conditions were stochastically sampled in this window according to their excitation probabilities. As explained in ref.[20], the trajectories ran for a maximum time of 1000 fs or until they reach an S_1/S_0 energy gap smaller than 0.1 eV. The latter condition due to limitations of the linear-response TDDFT to deal with S_1/S_0 degeneracies.[37]

All geometry optimizations at the MR-CISD level have been performed through analytical gradient techniques.[38-41] All MP2 calculations have been performed with the GAUSSIAN 09 software,[42] while all MCSCF, MR-CISD, and MR-CISD+Q calculations have been done with the COLUMBUS program system.[43-46] The DALTON program[47] has been used to compute the atomic orbitals (AO) integrals as well as the AO gradient

integrals used by COLUMBUS. The non-adiabatic dynamics calculations were performed using NEWTON-X[48, 49] interfaced with GAUSSIAN 09.[42]

3. Results and Discussion

3.1 Vertical Excitation

In Table 2, the vertical excitation energies, oscillator strengths (*f*), and the spatial extension of the CI wavefunction ($\langle r^2 \rangle$), as well as the CI weights of the main configurations are given. Comparison with previous results, obtained with the B1 basis set, is also provided.

Table 2. Vertical excitation energies (ΔE_v, in eV, at the MR-CISD+Q level), spatial extension ($\langle r^2 \rangle$), and oscillator strengths (*f*) for CF_3CH_2Cl obtained at the MR-CISD/*ref1* level with the B1 basis set.

State	ΔE_v (eV)		*f*	$\langle \mathbf{r}^2 \rangle$ (a_0^2)	Main configuration
	CI+Q	CI+Q[b,c]			
$1^1A'$	0.00	0.00	-	88.32	0.81(closed shell)
$2^1A'$	7.91	7.97	0.001	105.63	$0.60n_1\sigma^*+0.22n_1 4p_\sigma$
$3^1A'$	8.45	8.41	0.04855	132.37	$0.80n_1 4s$
$4^1A'$	9.23	9.19	0.01434	150.18	$0.83n_2 4p_2$
$5^1A'$	9.56	9.53	0.01331	154.42	$0.61n_1 4p_1 + 0.14n_1 4p_\sigma$
$6^1A'$	9.82	9.80	0.02443	159.14	$0.47n_1 4p_\sigma + 0.19n_1 4p_1 + 0.15\ n_1\sigma^*$
$7^1A'$	11.65	---	0.007107	131.74	$0.80\sigma 4s$
$8^1A'$	12.07	---	0.36092	149.58	$0.66\sigma 4p_\sigma + 0.13\sigma\sigma^*$
$9^1A'$	12.82	---	0.01575	165.67	$0.80\sigma 4p_1$
$1^1A''$	7.81	7.86	0.0006	105.60	$0.55n_2\sigma^*+0.23n_2 4p_\sigma$
$2^1A''$	8.33	8.29	0.03311	131.54	$0.76n_2 4s$
$3^1A''$	9.33	9.31	0.00094	150.36	$0.81n_1 4p_2$
$4^1A''$	9.49	9.45	0.01671	155.95	$0.69n_2 4p_1$
$5^1A''$	9.67	9.65	0.008831	158.76	$0.47n_2 4p_\sigma + 0.19n_2\sigma^*$
$6^1A''$	12.47	---	0.021108	151.05	$0.84\sigma 4p_2$

[a]Ground-state energies: -796.790689 (MR-CISD); -796.931224 (MR-CISD+Q); [b]From ref.[19]; [c]With the B4 basis set.

As can be seen from Table 2, there is an excellent agreement between the current results and those from ref.[19], with a maximum difference of only 0.05 eV. The primary weights are maintained, as can be seen through comparison between Table 1 and Table IV from ref.[19]. However, the results with the smaller basis set, B4, show a slightly larger

multiconfigurational character for some states. The energy differences between the A′ and A″ states arising from the same configuration (and involving excitation from the n orbitals) are in the range from 0.07 to 0.15 eV, and are compatible with the difference of 0.09 eV between the ionization potentials of the n_1 and n_2 lone pairs computed at the ROCCSD(T)/CBS level.[50]

As can also be seen from Table 2, the $\langle r^2 \rangle$ values lead to a clear separation between the valence (105 a_0^2) and Rydberg (132 - 159 a_0^2) states, although the $\langle r^2 \rangle$ values for the nσ* states are significantly larger than that of the ground state (88 a_0^2), due to a reasonable admixture with the n4pσ configuration.

The studied states of both CF_3CH_2Cl and CH_3Cl molecules are qualitatively analogous, as they have the same nature and energy ordering. Unsurprisingly, the quantitative variations are indeed not small due to the difference between the C–H and C–CF_3 bonds. For instance, the first two ionization potentials of the CF_3CH_2Cl molecule (both corresponding to ionization of Cl lone pairs) are 0.7 and 0.79 eV larger than those of the CH_3Cl molecule.[50, 51] The magnitude of such variation can also be seen in the differences between the excitation energies of these two molecules (both computed with the B1 basis set), as they can be as large as 0.85 eV (for the σ4p state), with the HCFC-133a molecule yielding larger values.

One central point of the present study is to demonstrate that, despite the quantitative variations mentioned, the similarities between CH_3Cl and CF_3CH_2Cl are strong enough so that one can expect a similar behavior for the latter based on what is observed for the former. Thus, some shared features by both molecules are: (i) the largest *f* value has been obtained for an n-*k*pσ state (with $k = 3$ for the CH_3Cl[23] and $k = 4$ for CF_3CH_2Cl), followed by an n-*k*s state (cf. Table 2 with Table 1 from ref.[23]); (ii) the vertical excitation energy into the n-*k*pσ state is very close to the vertical ionization potential; (iii) the potential energy curves along the C–Cl coordinate have similar topography; (iv) both molecules form the same type of ion pair, that is, a hydrogen-bonded contact ion pair. The points (iii) and (iv) will be discussed in sections 3.2 and 3.3, respectively.

3.2. Potential energy curves

In Figure 2, the potential energy curves along the C–Cl coordinate (relaxed scan in S_0) are shown. These curves share the following features with those from CH_3Cl:[23] (i)

they have the same crossings or avoided crossings between the n4p and σ4s/σ4p states; (ii) after ~ 2.3Å, the ionic configuration shows up in the $3^1A'$ state, and its weight increases until it becomes dominant from ~3.0 Å on (in the case of CH_3Cl, the corresponding state is 2^1A_1); (iii) around 3.2 Å, one has a partial minimum for the $3^1A'$ state, suggesting that it can become an actual minimum. In Figures S1 to S3 of the Supporting Information, the avoided crossings within the sets of A′ and A″ states are shown.

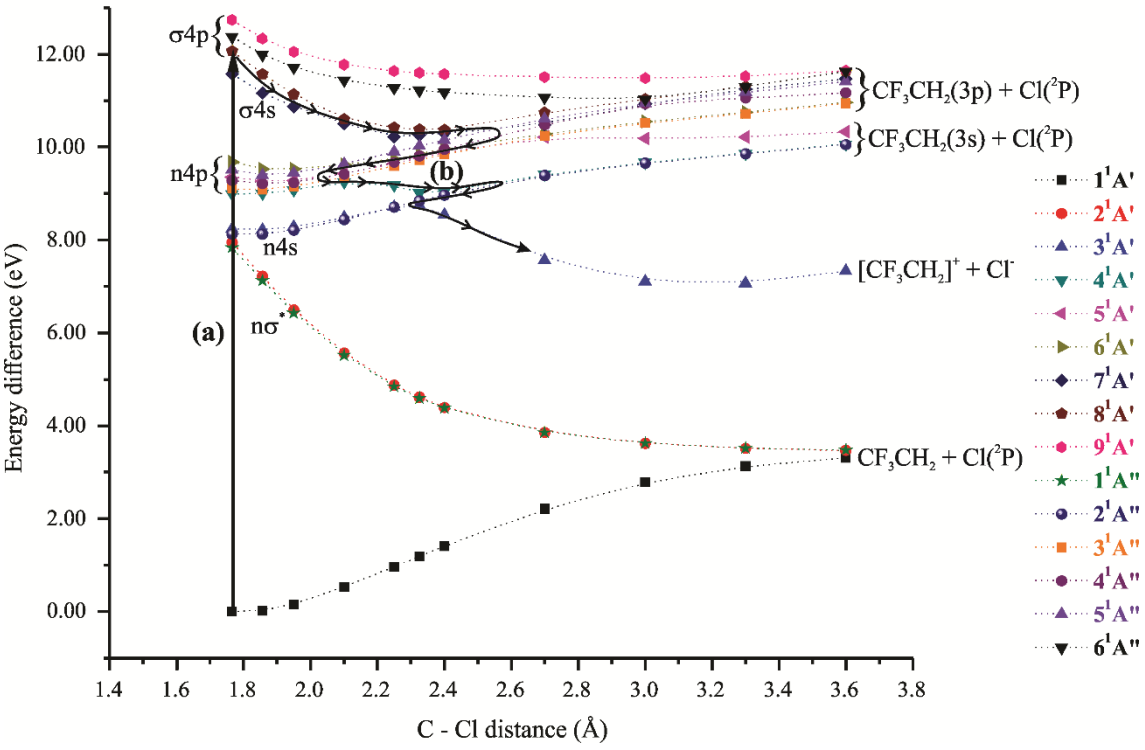

Figure 2. Potential energy curves for the C–Cl coordinate (relaxed scan in S_0) of the CF_3CH_2Cl molecule, computed at the MR-CISD/*ref1* level with the B1 basis set. The bold line indicates a possible pathway to relax to the ion-pair state, triggered by a vertical excitation into the state with the largest *f* value (the $8^1A'$ state).

The bold line in Figure 2 shows a possible pathway to relax into the ion-pair state, starting from the $8^1A'$ state, the one to which a vertical transition from the ground state has the largest *f* value (see Table 2). Such pathway can be induced by elongations and shortenings of the C–Cl bond and it consists of several nonadiabatic transitions, which can take place either maintaining or breaking the symmetry plane, depending on the pair of states involved. The first transition is from the $8^1A'$ to the $7^1A'$ state, which occurs at

~ 2.0 Å upon loss of the symmetry plane. The C–Cl bond elongation can proceed until ~ 2.55 Å, where the energy differences between the $7^1A'$ and the n4p states can decrease, inducing $7^1A' \rightarrow$ n4p transitions. A subsequent shortening of the C–Cl bond until ~ 2.05 Å can be accompanied by an energy decrease and by an approximation between n4p states, inducing a cascade of transitions until the lowest n4p state ($4^1A'$) is reached. Then, from this state, a further elongation of the C–Cl bond can decrease its energy and lead to a quasi-degeneracy between the $4^1A'$ and $2^1A''$ states. Finally, a further shortening can bring the $2^1A''$ and $3^1A'$ states near, inducing the final $2^1A'' \rightarrow 3^1A'$ transition. Once the $3^1A'$ state is reached, an elongation of the C–Cl bond stabilizes it (see Figure 2). This sequence of events is a simplified picture of the nonadiabatic transitions required to bring the system to the ion-pair state. A more detailed analysis of the time evolution of some geometrical parameters will be given in section 3.4.

3.3. Characterization of the hydrogen-bonded $CF_3HCH^+\cdots Cl^-$ ion pair

The relaxed scan shown in Figure 2 suggests the occurrence of a minimum for a C–Cl bond distance of ~ 3Å for the $3^1A'$ state. Thus, the corresponding structure resulting from this scan has been used as the initial guess for full geometry optimization of this state at the MR-CISD/*valence* level (see Table 1) with the B2 basis set. Although such calculation has been performed without symmetry, the obtained structure (shown in Figure 3(a)) virtually has C_s symmetry. Its normal mode analysis yields an imaginary frequency mode that breaks the C_s symmetry and decreases the $\angle_{CHCl}$ bond angle (that is, the Cl atom tends to become collinear with the C–H bond). After following this mode and performing a new geometry optimization, the structure shown in Figure 3(b) is obtained. The Cartesian coordinates of both structures are given in the Supporting Information, SI-3.

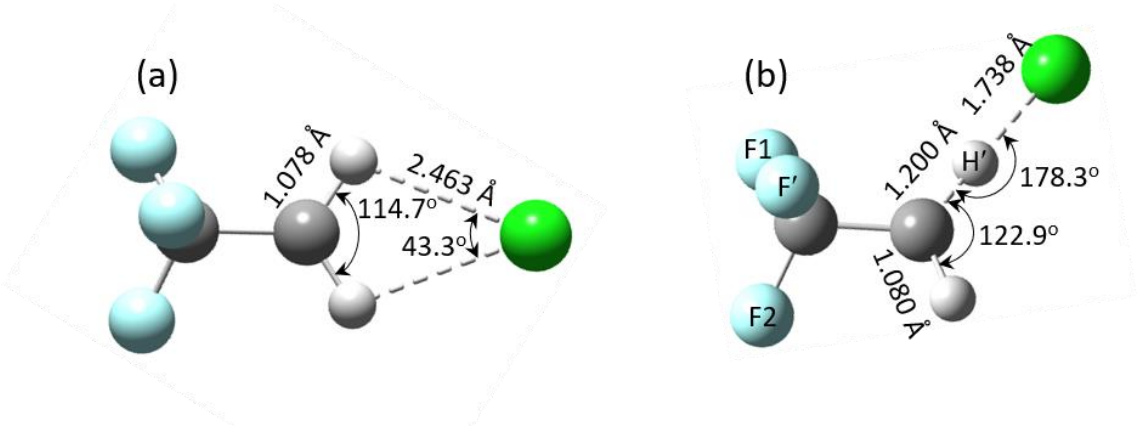

Figure 3. (a) Transition state resulting from the geometry optimization of the $3^1A'$ state based on the relaxed scan shown in Figure 2; (b) Structure of the hydrogen-bonded ion pair obtained for the $3^1A'$ state of the CF_3CH_2Cl molecule, computed at the MR-CISD/*valence* level with the B2 basis set. The main geometrical parameters are shown in the plot. F1 and F2 refer to the F atoms that are closer to the CCH′ and CCH planes, respectively.

A comparison between the C···H and H···Cl bond distances (along with the $\angle_{CHCl}$ bond angle, fragment charges, dipole moment and binding energy) computed for the CF_3CH_2Cl and the CH_3Cl molecules indicates similar hydrogen bonds. The C···H bond distance of the $CF_3HCH^+\cdots Cl^-$ ion pair is larger than that of the $H_2C^+H\cdots Cl^-$ ion pair by 0.042 Å. In turn, the H···Cl bond distance is smaller by 0.144 Å.

The charge separation in the $[CF_3CH_2]^{+\delta}Cl^{-\delta}$ ion pair, $\delta = 0.93$, is slightly larger than that in the ion $[CH_3]^{+\delta}Cl^{-\delta}$ pair, $\delta = 0.90$. The corresponding dipole moments are similar too, with values of 9.44 and 10.26 D, respectively. All these values have been obtained from single-point calculations (at the MR-CISD/*valence* level with the B3 basis set) performed on the optimized geometries. The binding energies of the $CF_3HCH^+\cdots Cl^-$ and $H_2CH^+\cdots Cl^-$ ion pairs are 4.30 and 3.53 eV, respectively, with the same basis at the MR-CISD+Q level. The difference of 0.77 eV between these two values can be partially explained by the inequivalent dissociated structures used as a reference to compute the binding energy. While CH_3Cl simply dissociates into $CH_3^+ + Cl^-$ in the ionic channel, in the same channel, dissociated HCFC-133a is further stabilized by an F migration, $CF_3C^+H_2 \rightarrow C^+F_2CFH_2$. Consequently, the energy of the ionic channel decreases, leading to smaller binding energy for the bonded ion pair. The F migration of $CF_3C^+H_2$ cation has

been previously characterized at the MP2 level.[32] Additional calculations at other correlated levels, along with previous results at the HF level, indicate that such spontaneous migration can only be captured at post-Hartree-Fock levels. The computed value of 10.78 eV for the vertical ionization potential (at the MP2/aug-cc-pVTZ level) is in excellent agreement with the experimental value of 10.6 eV given by Fisher *et. al.*[52]

The C^+–H···Cl^- moiety is a relatively uncommon structure. It has been reported in systems where the C atom is part of a heteroaromatic ring, and they are observed in the ground state.[53] In the most common systems, the C atom is part of an imidazolium ring, and the ion pairs are essential units of ionic liquids.[53-60] Due to the resonance structures, the positive charge center in these systems is shared between the C and two adjacent N atoms.[57] To the best of our knowledge, the hydrogen-bonded contact ion pair given in ref.[23], H_2CH^+···Cl^-, has been so far the only example of a molecule containing a C^+–H···Cl^- moiety in which the positive charge center (C^+) is part of an aliphatic backbone. The CF_3CH_2Cl molecule adds to this group as it shares the same two characteristics (presence of the C^+–H···Cl^- moiety and the positive charge center, C^+, as a part of an aliphatic backbone). For both CF_3CH_2Cl and CH_3Cl, however, the ion pairs are formed in the excited state.

The binding energy of 3.53 eV obtained here is close to the value of 4.07 eV obtained at the MP2 level for the hydrogen-bonded 1-ethyl-3-methylimidazolium chloride (EMIC) ion pair.[56] The same holds for the C–Cl distances obtained for both systems, which differ by just 0.087 Å, although for the latter, the H′Cl distance is longer by ~0.162 Å.[56] Compared to the value of 3.53 eV obtained for the CF_3HCH^+···Cl^- ion pair, the value of 4.07 eV for the EMIC ion pair is closer to the amount of 4.30 eV for the H_2CH^+···Cl^- ion pair. Such agreement can be explained by the absence of atom migration in this case, which reinforces the hypothesis that the F migration is essential for the destabilization of the CF_3HCH^+···Cl^- ion pair.

In Table 3, the computed vibrational frequencies of the hydrogen-bonded contact ion-pair, CF_3HCH^+···Cl^- (structure (b) in Figure 3), are given. As the normal coordinates differ significantly from those of the $[H_2C^+H]Cl^-$ ion pair as well as from those of the ground state of the CF_3CH_2Cl molecule they cannot be directly compared.

Table 3. Vibrational frequencies (in cm^{-1}) for the $CF_3HCH^+\cdots Cl^-$ hydrogen-bonded contact ion pair, obtained at the MR-CISD/valence level with the B2 basis set. For the atoms' labeling see Figure 3(b).

ν (cm^{-1})	Approximate description
35.4	CH′Cl out-of-plane bending[a] coupled to F1CC and CCH bending
71.9	C–H′ stretching coupled to H′Cl stretching and to CFF′ twisting
286.5	CH′Cl out-of-plane bending[a] coupled to F′CC and CCH bending.
304.7	CH′Cl out-of-plane bending[a] coupled to H′Cl and CH stretching and to CF1F2 twisting
470.9	symmetric CH_2 stretching coupled to H′Cl stretching, to antisymmetric CF2F′ stretching and to CF1F′ bending
540.0	CH_2 twisting coupled to CF_2 antisymmetric stretching
558.1	asymmetric CH_2 stretching coupled to H′Cl stretching and CF1F′ bending
619.1	CH_2 twisting coupled to H′Cl, C – C and CF1F′ symmetric stretching
766.9	out-of-plane CH′Cl bending[a]
894.8	F1CCH rotation coupled to CF1F′ twisting and bending and to CH′ and H′Cl stretching
1010.7	H′Cl stretching coupled to CH′ stretching and in-plane CH′Cl bending[a]
1227.0	CH_2 wagging
1336.8	symmetric CH_2 stretching coupled to F′CC twisting
1368.4	CH′Cl (in phase) stretching coupled to CCF′ twisting
1500.9	out-of-plane CH′Cl bending[a]
1531.7	CH′ stretching anti-symmetrically (out-of-phase) coupled to H′Cl stretching and symmetrically coupled to C – C stretching and also coupled to nearly in-plane CH′Cl bending[a]
1750.3	CH′ stretching anti-symmetrically (out-of-phase) coupled to H′Cl and C–C stretching and also coupled to nearly in-plane CH′Cl bending[a]
3300.6	in-plane CH′Cl bending[a] coupled to CH′ and H′Cl stretching

[a]The two different modes with the same description have the atomic displacements in opposite directions of the CCH plane (see also Table S3 of the Supporting Information). The plane used to define the in-plane and out-of-plane CH′Cl bending vibrations is the one defined by the HCCl atoms.

Although inclusion of the chloride anion increases the number of vibrational modes by three, the frequencies of the ion pair are better described regarding how the added anion modifies the cation frequencies. Nevertheless, the F migration prevents such comparison, as the formed $C^+F_2CFH_2$ carbocation is not able to form any hydrogen bond with chloride. Still, the first two vibrational modes (in the far infrared region) are

consistent with the corresponding modes observed in trialkyl ammonium salts.[61] For these salts, the highest and the lowest frequencies (in the far infrared region) have been respectively assigned to the cation-anion stretching mode and to the N^+–H···Cl^- bending mode, which is consistent with the description given in Table 3 for the vibrational modes whose frequencies are 71.9 and 35.4 cm^{-1}. The highest frequency CH′ stretching mode has a vibrational frequency of 1750.3 cm^{-1} (see Table 3 and Figure 3(b)), a value much smaller than the one obtained for the hydrogen-bonded 1-Butyl-3-methylimidazolium chloride, 2655 cm^{-1}.[57] This significant difference can be explained by the longer CH′ bond distance obtained here (1.200 versus 1.111 Å[59]) and by its coupling with two lower frequency modes, that is, the C–C stretching mode and the in-plane CH′Cl bending mode. "Pure" C–C stretching frequencies are observed at ~ 800–1200 cm^{-1}.[62] Although a "pure" in-plane CH′Cl bending mode has not been obtained here, it is expected that its frequency is close to one of the two frequencies of the out-of-plane CH′Cl bending modes, observed at 766.9 and 1500.9 cm^{-1} (see Table 3). The relative displacement vectors for each normal mode are given in Table S3 of the Supporting Information.

3.3 Nonadiabatic dynamics

In the previous sections, we have argued that after a high-energy excitation of CF_3CH_2Cl, a cascade of nonadiabatic events should produce Cl^- fragments through the population of the ion-pair state. To verify this hypothesis, we have run on-the-fly nonadiabatic dynamics simulations.

As mentioned in the Introduction, the computational costs of those simulations at MR-CISD level are prohibitive. For this reason, we resorted to linear-response TDDFT, which can adequately describe the topography of the states of interest at a much lower cost. The critical point for such methodological shift is how well the TDDFT potential energies compare to those computed with MR-CISD.

In fact, we have already addressed this issue in ref.[20], where we reported TDDFT dynamics for CF_3CH_2Cl. The TDDFT calculations with the ωB97XD functional lead to a good description of the potential energy curves of the CF_3CH_2Cl molecule along the C–Cl coordinate, as can be seen through comparison between Figure (b) from Table S2 of ref.[20] and Figure 2. The main features correctly described at the TDDFT/ωB97XD level are: (i) the separation between the groups of nσ*, σ4s, and σ4p states in the region before

~2.1 Å; (ii) the crossing between the n4s and the $3^1A'$ states upon C–Cl elongation ($3^1A'$ becomes the ion-pair state upon elongation of the C–Cl bond); (iii) the relatively close proximity between states S_4 to S_{14} in the region between ~ 2.6 and 3.6 Å), within a relatively narrow range of ~ 2.5 eV (from ~ 9.5 to 12 eV). Although Figure (b) of Table S2 of ref.[20] does not suggest the formation of a minimum in the fourth surface, after full geometry optimization of this state at the TDDFT/ωB97XD level (with the B4 basis set) a minimum, whose structure is similar to that shown in Figure 3(b), is obtained. Its Cartesian coordinates are given in Table S2 of the Supporting Information.

In ref.[20], the nonadiabatic dynamics calculations were performed exciting the molecule in a spectral window at 10.0 ± 0.25 eV. A closer look at the results used to generate Table 3 of ref.[20] indicates that 4 out of the 28 trajectories that yielded Cl fragments (from a total of 100 trajectories) ended up in the fourth surface (S_3), whose associated electronic configuration indicates the formation of the $[CF_3CH_2]^+$ and Cl^- ions. Therefore, considering the statistical uncertainty for a confidence interval of 95%, the Cl^- yield is 4 ± 3% at the 10.0 ± 0.25 eV excitation energy window.

There are four pieces of information that inspired us to run new nonadiabatic dynamics calculations for CF_3CH_2Cl, but now using a spectral window at 11.2± 0.25 eV: (i) The Cl^- generated from CH_3Cl in the vacuum-UV photoexcitation experiments performed by Tuckett *et al.*[21, 22] has its largest yield in the range extending from ~ 10.75 to 11.75 eV. (ii) Results from ref.[23] indicate that a $\sigma 3p_\sigma$ state is the state with the largest oscillator strength in this region. Besides, it is also the state with the largest oscillator strength among all computed states.[23] (iii) For CF_3CH_2Cl, the same type of state ($\sigma 4p_\sigma$) is the one with the largest oscillator strength among all computed states, at both MR-CISD (see Table 2) and TDDFT/ωB95XD levels. (iv) At this latter level, the excitation energy of the $\sigma 4p_\sigma$ state is 11.2 eV. Therefore, we expected that nonadiabatic dynamics in a spectral window at 11.2 ± 0.25 eV should increase the Cl^- yield, as compared to that performed at the 10.0 ± 0.25 eV spectral window.[20]

In fact, in the new set of dynamics simulations, fifteen out of 100 trajectories ended in the S_3 ion-pair state, corresponding to a Cl^- yield of 15 ± 6% at the excitation energy window of 11.2 ± 0.25 eV, an almost three times bigger yield than in the lower excitation window.[20] In the following, we will focus the analysis exclusively on these fifteen trajectories yielding the ion pair.

The time elapsed for the system to reach S_3 varies from 35 to 244 fs (mean value of 150 fs with 70 fs standard deviation), and once this surface is reached, the system remains on it until the end of the dynamics. Figure 4 shows a typical example. As explained in the Computational Details, for methodological reasons, trajectories were finished as soon as the S_0/S_1 energy gap became smaller than 0.1 eV, and this criterion was always satisfied within a time interval varying between 5 and 56.5 fs after reaching S_3. The occurrence of an S_1/S_0 degeneracy with the system still in S_3 is not surprising given the semi-dissociated configuration of the molecule.

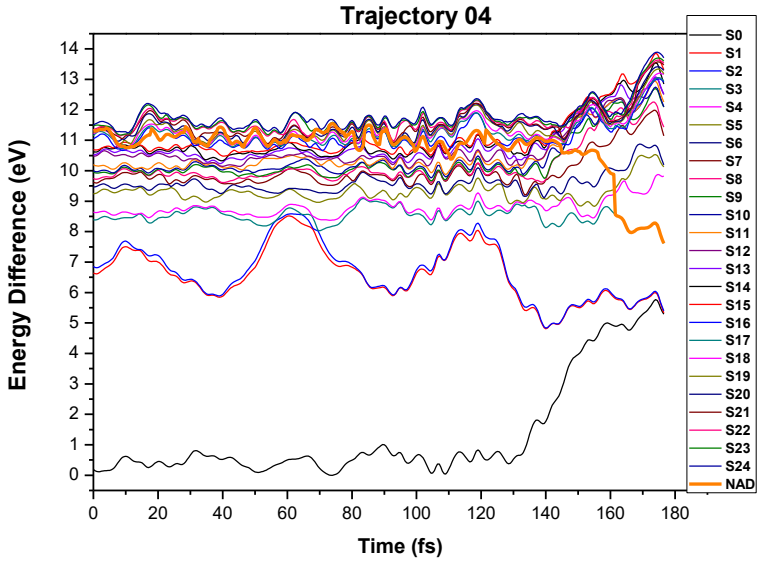

Figure 4. Time evolution of the potential energy surfaces for one of the fifteen trajectories that ended up in S_3. NAD stands for the actual state where the system is at each time step.

Figure 5 shows the time evolution of the C–Cl distance for the fifteen trajectories ending up in S_3. As can be seen from this plot, S_3 is always reached when the C–Cl distance is larger than 2.0 Å. Besides, some oscillations are observed for most of the trajectories, which is in line with the simplified pathway shown in Figure 2. The trajectories hoped to S_3 with an average C–Cl distance of 2.61 Å and with a standard deviation of 0.36 Å.

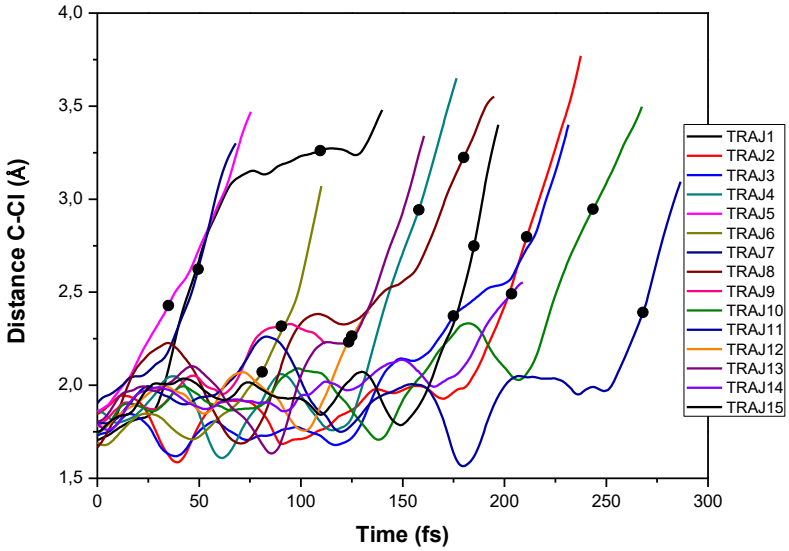

Figure 5. Time evolution of the C–Cl distance for the fifteen trajectories which end up in S_3. The black circles indicate the time elapsed when S_3 is reached.

As shown in Figure 6, the 15 trajectories populating the ion-pair state reach S_3 near the symmetric structure (Figure 3(a)), although with a broad spread of H–Cl distances, spanning from 2.5 to 3.5 Å. Due to the short period that they remain on S_3 before reaching the termination criterion, it is not possible to observe the formation of the H-bond (in Figure 6, they would be represented by periodic motions around the (b) structures). Nevertheless, we see that most of the trajectories depart from the symmetric structure immediately after hopping to S_3, as expected. At this point it is not possible to tell whether following this evolution, the trajectories will quickly yield Cl^- or stabilize in the ion-pair H-bond well. Given the considerable excess vibrational energy due to the nonadiabatic relaxation, the first option seems to be likely.

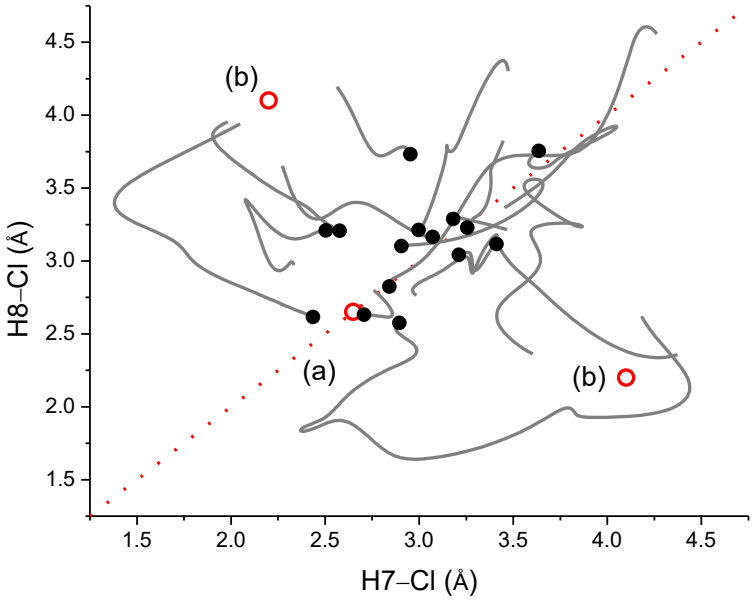

Figure 6. Time evolution of each the H–Cl distance for each of the fifteen trajectories reaching the ion-pair state. The black dot indicates the time in which the trajectory hops to S_3. The open circles show the same types of ion pair structures shown in Figure 3(a) and Figure 3(b), but optimized with TDDFT.

Conclusions

The hydrogen-bonded contact ion pair of the CF_3CH_2Cl molecule has been studied at the highly correlated MR-CISD level, including extensivity corrections. Its structure can be represented by $CF_3HCH^+\cdots Cl^-$. Our results indicate an extremely polar structure with a dipole moment of 10.26 D and binding energy of 3.53 eV. This energy is 0.77 eV lower than that of the prototype $H_2C^+H\cdots Cl^-$ system, a difference that can be explained by the additional stabilization of the $CF_3C^+H_2$ carbocation due to the F migration, $CF_3C^+H_2 \rightarrow C^+F_2CFH_2$.

Potential energy curve calculations along the C–Cl coordinate have also been performed to analyze the formation of the ion-pair state from the vertical excitation to the $\sigma 4p_\sigma$ state, the one with the largest *f* value. Such formation is based on several nonadiabatic transitions induced by C–Cl elongations and shortenings.

Despite the stability of the $CF_3HCH^+\cdots Cl^-$ structure, it should have a short lifetime, as electronic to vibrational energy conversion during population transfer to the ion-pair state is likely to populate excited low-frequency vibrational levels, which can release Cl^-

or HCl. The detection of the $CF_3HCH^+\cdots Cl^-$ ion pair can be carried out through the same technique[63] suggest to detect the related $H_2CH^+\cdots Cl^-$ ion pair.[23]

Nonadiabatic dynamics calculations at the TDDFT/ωB97XD level along with the potential energy profiles computed at the MR-CISD level suggest the release of Cl^- through a pathway following the potential energy surface of the ion-pair state, analogous to that followed by CH_3Cl. The ion-pair state is populated within the sub-picosecond scale (about 150 fs) and its yield depends on the excitation energy. An increase in the excitation window from 10.0 ± 0.25 eV to 11.2 ± 0.25 eV (reaching the $\sigma 4p_\sigma$ state) leads to an increase from 4 to 15% in the Cl^- yield.

At the highest computational level (MR-CISD+Q), the vertical excitation energy of the $\sigma 4p_\sigma$ state is 12.0 eV (103.3 nm). As the transition to this state is the one with the largest *f* value, to facilitate Cl^- release from the HCFC-133a molecule, we suggest studying its photodissociation at a wavelength close to 103 nm.

Finally, Cl^- release can in principle take place in related compounds, as some chloro-carbonyl compounds,[64-67] as long as: (i) the R-CH_2 and Cl open-shell doublet radicals are present not very far from each other, during photodissociation of the parent compound; and (ii) the excitation energy is high enough to achieve the ion pair channel.

ASSOCIATED CONTENT

Supporting Information

The Supporting Information is available free of charge on the ACS Publications website.

Potential energy curves; Cartesian coordinates; Displacement vectors of the normal modes; Molecular orbitals; Discussion on the basis sets choice.

AUTHOR INFORMATION

Corresponding authors

* E-mail: mario.barbatti@univ-amu.fr; website: www.barbatti.org

* E-mail: silmar@quimica.ufpb.br or silmar.monte@uol.com.br

ORCID

Gessenildo P. Rodrigues: 0000-0002-1166-9231

Thayana Maria Lopes de Lima: 0000-0001-8648-2108

Railton B. de Andrade: 0000-0001-5804-4186

Elizete Ventura: 0000-0002-1015-7824

Silmar A. do Monte: 0000-0002-5878-1984

Mario Barbatti: 0000-0001-9336-6607

Acknowledgment

M.B. thanks the support of the Excellence Initiative of Aix-Marseille University (A*MIDEX) and the project Equip@Meso (ANR-10-EQPX-29-01), both funded by the French Government "Investissements d'Avenir" program m. M.B. also acknowledges funding the WSPLIT project (ANR-17-CE05-0005-01). E.V. thanks the support of the Brazilian agency CNPq (Grant number 309785/2015-4). The remaining authors are grateful of the Brazilian agencies CAPES and FINEP for financial support. They are also thankful for the computational facilities at the CESUP/UFRGS supercomputing center.

Notes

The authors declare no competing financial interest.

References

1. Seinfeld, J. H.; Pandis, S. N. *Atmospheric Chemistry and Physics: From Air Pollution to Climate Change*. Willey: 2016.

2. Society, A. C. Which Gases Are Greenhouse Gases? ACS Climate Science Toolkit | Greenhouse Gases. https://www.acs.org/content/acs/en/climatescience/greenhousegases/whichgases.html.

3. *Kyoto Protocol to the United Nations Framework Convention on Climate Change*; Kyoto, 1997.

4. Downie, D. L., *Stratospheric Ozone Depletion*. Routledge: New York, 2013.

5. Downie, D. L. *The Vienna Convention, Montreal Protocol and Global Policy to Protect Stratospheric Ozone*. Taylor & Francis: Oxford, U.K., 2012.

6. Andersen, S. O.; Sarma, K. M.; Taddonio, K. N. *Technology Transfer for the Ozone Layer: Lessons for Climate Change*. Earthscan Press: London, 2007.

7. Andersen, S. O.; Sarma, K. M. *Protecting the Ozone Layer: the United Nations History*. Earthscan Press: London, 2002.

8. *Report of the Fourth Meeting of the Parties to the Montreal Protocol on Substances that Deplete the Ozone Layer*; United Nations Environment Panel: New York, 1992.

9. Miller, M.; Batchelor, T. Information Paper on Feedstock Uses of Ozone-Depleting Substances. [http://ec.europa.eu/clima/policies/ozone/research/docs/feedstock_en.pdf]. **2012**, 72.

10. Manzer, L. E. The CFC-Ozone Issue: Progress on the Development of Alternatives to CFCs. *Science* **1990,** *249*, 31-35.

11. Laube, J. C.; Newland, M. J.; Hogan, C.; Brenninkmeijer, C. A. M.; Fraser, P. J.; Martinerie, P.; Oram, D. E.; Reeves, C. E.; Röckmann, T.; Schwander, J.; et al. Newly Detected Ozone-Depleting Substances in the Atmosphere. *Nat. Geosci.* **2014,** *7*, 266-269.

12. McGillen, M. R.; Bernard, F.; Fleming, E. L.; Burkholder, J. B. HCFC-133a (CF_3CH_2Cl): OH Rate Coefficient, UV and Infrared Absorption Spectra, and Atmospheric Implications. *Geophys. Res. Lett.* **2015,** *42*, 6098-6105.

13. Setser, D. W.; Lee, T. S.; Danen, W. C. Infrared Multiphoton Absorption and Reaction of 2-Chloro-1,1,1 trifluoroethane. *J. Phys.Chem.* **1985,** *89*, 5799−5805.

14. Rakestraw, D. J.; Holmes, B. E. Unimolecular Rate Constants for Chemically Activated 1,1,1-Trifluoro-2-chloroethane: A Competitive Three-Channel System. *J. Phys. Chem.* **1991,** *95*, 3968−3975.

15. Enstice, E. C.; Duncan, J. R.; Setser, D. W.; Holmes, B. E. Unimolecular Reactions in the $CF_3CH_2Cl \leftrightarrow CF_2ClCH_2F$ System: Isomerization by Interchange of Cl and F Atoms. *J. Phys. Chem. A.* **2010,** *115*, 1054−1072.

16. Wang, L.; Zhao, Y.; Zhang, J.; Dai, Y.; Zhang, J. Dual-Level Direct Dynamics Studies on the Hydrogen Abstraction Reactions of Fluorine Atoms with CF_3CH_2X(X = F, Cl). *Theor. Chem. Acc.* **2011,** *128*, 183-199.

17. Zhao, Y.; He, H.; Zhang, J.; Wang, L. Direct Dynamics Study of the Hydrogen Abstraction Reaction of $CF_3CH_2Cl + Cl \rightarrow CF_3CHCl + HCl$. *Int. J. Chem. Kinet.* **2012,** *44*, 661-667.

18. Ichimura, T.; Kirk, A. W.; Tschuikow-Roux, E. Primary Processes in the 147- and 123.6-nm Photolyses of 1,1,1-Trifluoro-2-chloroethane. *J. Phys. Chem.* **1977,** *81*, 1153-1156.

19. Rodrigues, G. P.; Lucena Jr., J. R.; Ventura, E.; do Monte, S. A.; Reva, I.; Fausto, R. Matrix Isolation Infrared Spectroscopic and Theoretical Study of 1,1,1-trifluoro-2-chloroethane (HCFC-133a). *J. Chem. Phys.* **2013,** *139*, 204302-204310.

20. Rodrigues, G. P.; Ventura, E.; do Monte, S. A.; Barbatti, M. Photochemical Deactivation Process of HCFC-133a ($C_2H_2F_3Cl$): A Nonadiabatic Dynamics Study. *J. Phys. Chem. A.* **2014,** *118*, 12041−12049.

21. Simpson, M. J.; Tuckett, R. P. Vacuum-UV Negative Photoion Spectroscopy of Gas-Phase Polyatomic Molecules. *Int. Rev. Phys. Chem.* **2011,** *30*, 197-273.

22. Rogers, N. J.; Simpson, M. J.; Tuckett, R. P.; Dunn, K. F.; Latimer, C. J. Vacuum-UV Negative Photoion Spectroscopy of CH_3F, CH_3Cl and CH_3Br. *Phys. Chem. Chem. Phys.* **2010,** *12*, 10971–10980.

23. De Medeiros, V. C.; De Andrade, R. B.; Leitão, E. F. V.; Ventura, E.; Bauerfeldt, G. F.; Barbatti, M.; Do Monte, S. A. Photochemistry of CH_3Cl: Dissociation and CH···Cl Hydrogen Bond Formation. *J. Am. Chem. Soc.* **2016,** *138*, 272-280.

24. Crespo-Otero, R.; Barbatti, M. Recent Advances and Perspectives on Nonadiabatics Mixed Quantum-Classic Dynamics. *Chem. Rev.* **2018,** *118*, 7026-7068.

25. Kendall, R. A.; Dunning, T. H., Jr.; Harrison, R. J. Electron Affinities of the First-Row Atoms Revisited. Systematic Basis Sets and Wave Functions. *J. Chem. Phys.* **1992,** *96*, 6796−6807.

26. De Medeiros, V. C.; Ventura, E.; do Monte, S. A. CASSCF and MR−CISD Study of the n-4s and n-4pe Rydberg States of the CF_3Cl. *Chem. Phys. Lett.* **2012,** *546*, 30-33.

27. Lucena, J. R., Jr.; Ventura, E.; do Monte, S. A.; Araújo, R. C. M. U.; Ramos, M. N.; Fausto, R. Dissociation of Ground and nσ* States of CF_3Cl Using Multireference Configuration Interaction with Singles and Doubles and with Multireference Average Quadratic Coupled Cluster Extensivity Corrections. . *J. Chem. Phys.* **2007,** *127*, 164320-164330.

28. Bunge, A. Electronic Wavefunctions for Atoms III. Partition of Degenerate Spaces and Ground State of C. *J. Chem. Phys.* **1970,** *53*, 20-28.

29. Langhoff, S. R.; Davidson, E. R. Configuration Interaction Calculations on Nitrogen Molecule. *Int. J. Quantum Chem.* **1974,** *8*, 61-72.

30. Bruna, P. J.; Peyerimhoff, S. D.; Buenker, R. J. The Ground-State of the CN^+ Ion - a Multi-Reference CI Study. *Chem. Phys. Lett.* **1980,** *72*, 278-284.

31. De Medeiros, V. C.; De Andrade, R. B.; Rodrigues, G. P.; Bauerfeldt, G. F.; Ventura, E.; Barbatti, M.; Do Monte, S. A. Photochemistry of CF_3Cl: Quenching of Charged Fragments Is Caused by Nonadiabatic Effects. *J. Chem. Theory Comput.* **2018,** *14*, 4844–4855.

32. Gronert, S.; Keefe, J. R. Calculated Stabilities and Structures for Carbocations and Singlet Carbenes Bearing Electron-Withdrawing Groups. *J. Phys. Org. Chem.* **2013,** *26*, 1023–1031.

33. Tully, J. C. Nonadiabatic Molecular Dynamics. *Int. J. Quantum Chem.: Quantum Chem. Simposium* **1991,** *25*, 299-309.

34. Granucci, G.; Persico, M. Critical Appraisal of the Fewest Switches Algorithm for Surface Hopping. *J. Chem. Phys.* **2007,** *126*, 134114.

35. Barbatti, M.; Pittner, J.; Pederzoli, M.; Werner, U.; Mitrić, R.; Bonačić-Koutecký, V.; Lischka, H. Non-Adiabatic Dynamics of Pyrrole: Dependence of Deactivation Mechanisms on the Excitation Energy. *Chem. Phys.* **2010,** *375*, 26-34.

36. Chai, J.-D.; Head-Gordon, M. Long-Range Corrected Hybrid Density Functionals with Damped Atom−Atom Dispersion Corrections. *Phys. Chem. Chem. Phys.* **2008,** *10*, 6615−6620.

37. Plasser, F.; Crespo-Otero, R.; Pederzoli, M.; Pittner, J.; Lischka, H.; Barbatti, M. Surface Hopping Dynamics with Correlated Single-Reference Methods: 9H-Adenine as a Case Study. *J. Chem. Theory Comput.* **2014,** *10*, 1395−1405.

38. Shepard, R.; Lischka, H.; Szalay, P. G.; Kovar, T.; Ernzerhof, M. A General Multireference Configuration-Interaction Gradient Program. *J. Chem. Phys.* **1992,** *96*, 2085−2098.

39. Shepard, R. The Analytic Gradient Method for Configuration Interaction Wave Functions. *In Modern Electronic Structure Theory; Yarkony, D. R., Ed.; World Scientific: Singapore* **1995,** *1*, 245.

40. Shepard, R. Geometrical Energy Derivative Evaluation with MRCI Wave Functions. *Int. J. Quantum Chem.* **1987,** *31*, 33-34.

41. Lischka, H.; Dallos, M.; Shepard, R. Analytic MRCI Gradient for Excited States: Formalism and Application to the n-π* Valence and n-(3s,3p) Rydberg States of Formaldehyde. *Mol. Phys.* **2002,** *100*, 1647-1658.

42. Frisch, M. J.; Trucks, G. W.; Schlegel, H. B.; Scuseria, G. E.; Robb, M. A.; Cheeseman, J. R.; Scalmani, G.; Barone, V.; Mennucci, B.; Petersson, G. A.; et al, Gaussian 09, Revision D.01; Gaussian, Inc.: Wallingford, CT,. **2013**.

43. Shepard, R.; Shavitt, I.; Pitzer, R. M.; Comeau, D. C.; Pepper, M.; Lischka, H.; Szalay, P. G.; Ahlrichs, R.; Brown, F. B.; Zhao, J. A Progress Report on the Status of the COLUMBUS MRCI Program System. *Int. J. Quantum Chem.* **1988,** *34*, 149-165.

44. Lischka, H.; Shepard, R.; Shavitt, I.; Pitzer, R. M.; Dallos, M.; Müller, T.; Szalay, P. G.; Brown, F. B.; Ahlrichs, R.; Böhm, H. J.; et al. COLUMBUS, an Ab Initio Electronic Structure Program, Release 7.0. www.univie.ac.at/columbus (accessed September 4, 2018).

45. Lischka, H.; Shepard, R.; Pitzer, R. M.; Shavitt, I.; Dallos, M.; Müller, T.; Szalay, P. G.; Seth, M.; Kedziora, G. S.; Yabushita, S.; et al. New High-Level Multireference Methods in the Quantum-Chemistry Program System COLUMBUS: Analytic MR-CISD and MR-AQCC Gradients and MR-AQCC-LRT for Excited States, GUGA Spin-Orbit CI, and Parallel CI Density. *Phys. Chem. Chem. Phys.* **2001,** *3*, 664-673.

46. Lischka, H.; Shepard, R.; Brown, F. B.; Shavitt, I. New Implementation of the Graphical Unitary-Group Approach for Multi-Reference Direct Configuration-Interaction Calculations. *Int. J. Quantum Chem.* **1981,** *20*, 91-100.

47. Helgaker, T.; Jensen, H. J. A.; Jørgensen, P.; Olsen, J.; Ruud, K.; Ågren, H.; Andersen, T.; Bak, K. L.; Bakken, V.; Christiansen, O.; et al. DALTON, an Ab Initio Electronic Structure Program, Release 1.0. **1997**.

48. Barbatti, M.; Ruckenbauer, M.; Plasser, F.; Pittner, J.; Granucci, G.; Persico, M.; Lischka, H. Newton-X: A Surface-Hopping Program for Nonadiabatic Molecular Dynamics. *WIREs: Comp. Mol. Sci.* **2014,** *4*, 26-33.

49. Barbatti, M.; Granucci, G.; Ruckenbauer, M.; Plasser, F.; Crespo-Otero, R.; Pittner, J.; Persico, M.; Lischka, H. NEWTON-X: A package for Newtonian Dynamics Close to the Crossing Seam. Available via the Internet at www.newtonx.org. **2018**.

50. Rodrigues, G. P.; Lucena, J., Jr.; Ventura, E.; do Monte, S. A. Accurate Calculation of the Ionization Energies of the Chlorine Lone Pairs in 1,1,1-trifluoro-2-chloroethane (HCFC-133a). *J. Mol. Model.* **2014,** *20*, 2393-2400.

51. Karlsson, L.; Jadrny, R.; Mattsson, L.; Chau, F. T.; Siegbahn, K. Vibrational and Vibronic Structure in the Valence Electron Spectra of CH_3X Molecules (X=F, CI, Br, I, OH). *Phys. Scr.* **1977,** *16*, 225-234.

52. Fisher, I. P.; Homer, J. B.; Lossing, F. P. Free Radicals by Mass Spectrometry. XXXIII. Ionization Potentials of CF_2, CF_3CF_2, CF_3CH_2, n-C_3F_7 and i-C_3F_7 Radicals. *J. Am. Chem. Soc.* **1965,** *87*, 957−960.

53. Cai, J.; Sessler, J. L. Neutral CH and Cationic CH Donor Groups as Anion Receptors. *Chem. Soc. Rev.* **2014,** *43*, 6198−6213.

54. Matthews, R. P.; Ashworth, C.; Welton, T.; Hunt, P. A. The Impact of Anion Electronic Structure: Similarities and Differences in Imidazolium Based Ionic Liquids. *J. Phys.: Condens. Matter* **2014,** *26*, 284112.

55. Lungwitz, R.; Spange, S. A Hydrogen Bond Accepting (HBA) Scale for Anions, Including Room Temperature Ionic Liquids. *New J. Chem.* **2008,** *32*, 392–394.

56. Izgorodina, E. I.; MacFarlane, D. R. Nature of Hydrogen Bonding in Charged Hydrogen-Bonded Complexes and Imidazolium-Based Ionic Liquids. *J. Phys. Chem. B* **2011,** *115*, 14659–14667.

57. Hunt, P. A.; Kirchner, B.; Welton, T. Characterising the Electronic Structure of Ionic Liquids: An Examination of the 1-Butyl-3-Methylimidazolium Chloride Ion Pair. *Chem. Eur. J.* **2006,** *12*, 6762-6775.

58. Hunt, P. A.; Gould, R.; Kirchner, B. The Structure of Imidazolium-Based Ionic Liquids: Insights from Ion-Pair Interactions. *Aust. J. Chem.* **2007,** *60*, 9-14.

59. Hunt, P. A.; Gould, I. R. Structural Characterization of the 1-Butyl-3-Methylimidazolium Chloride Ion Pair Using Ab Initio Methods. *J. Phys. Chem. A.* **2006,** *110*, 2269-2282.

60. Dymek, C. J.; Grossie, D. A.; Fratini, A. V.; Adams, W. W. Evidence for the Presence of Hydrogen-Bonded Ion-Ion Interactions in the Molten Salt Precursor, 1-methyl-3-ethylimidazolium chloride. *J. Mol. Struct.* **1989,** *213*, 25-34.

61. Kludt, J. R.; Kwong, G. Y. W.; McDonald, R. L. Far Infrared Spectra of Tertiary Ammonium Salts. *J. Phys. Chem.* **1972,** *76*, 339–342.

62. Silverstein, R. M.; Webster, F. X.; Kiemle, D. J. *Spectrometric Identification of Organic Compounds*. 7th ed.; John Wiley & Sons: NJ, USA, 2005.

63. Jonas, D. M. Two-Dimensional Femtosecond Spectroscopy. *Annu. Rev. Phys. Chem.* **2003,** *54*, 425–463.

64. Adams, J. D.; Scrape, P. G.; Li, S.; Li, S.-H.; Butler, L. J. Primary Product Branching in the Photodissociation of Chloroacethaldehyde at 157 nm. *J. Phys. Chem. A.* **2017,** *121*, 6732–6741.

65. Cui, G.; Sun, Z.; Fang, W. Adiabatic and Nonadiabatic Bond Cleavages in Norrish Type I Reaction. *J. Phys. Chem. A.* **2011,** *115*, 10146 – 10153.

66. Cui, G.-L.; Li, Q.-S.; Zhang, F.; Fang, W.-H.; Yu, J.-G. Combined CASSCF and MR-CI Study on Photoinduced Dissociation and Isomerization of Acryloyl Chloride. *J. Phys. Chem. A.* **2006,** *110*, 11839 – 11846.

67. Lam, C.-S.; Adams, J. D.; Butler, L. J. The Onset of H + Ketene Products from Vinoxy Radicals Prepared by Photodissociation of Chloroacetaldehyde at 157 nm. *J. Phys. Chem. A.* **2016,** *120*, 2521 – 2536.

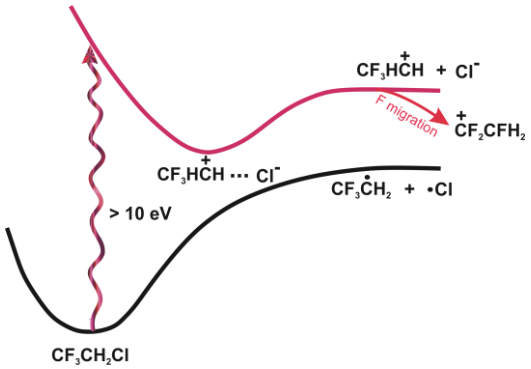
$CF_3\overset{+}{H}CH + Cl^-$
F migration
$CF_2\overset{+}{C}FH_2$
$CF_3\overset{+}{H}CH \cdots Cl^-$
$CF_3\dot{C}H_2 + \bullet Cl$
> 10 eV
CF_3CH_2Cl